

# Flow-Mach-number-induced hysteresis phenomena in the interaction of conical shock waves – a numerical investigation

By G. BEN-DOR<sup>1</sup>, T. ELPERIN<sup>1</sup> AND E. I. VASILIEV<sup>2</sup>

<sup>1</sup>Pearlstone Center for Aeronautical Engineering Studies, Department of Mechanical Engineering, Ben-Gurion University of the Negev, Beer Sheva, Israel

<sup>2</sup>Department of Computational Mechanics, Volgograd State University, Volgograd, Russia

(Received 25 October 2001 and in revised form 17 July 2003)

A flow-Mach-number-induced hysteresis phenomenon, in the shock-on-shock interaction of conical shock waves, is investigated numerically, by solving the Euler equations, using a W-modification of the non-stationary Godunov method with second-order accuracy both in space and time. The investigation reveals a multi-path hysteresis loop. It is shown that there are flow Mach number ranges in which three different wave configurations can be obtained for identical flow conditions. This study complements an earlier study by Ben-Dor *et al.* (2001) in which an angle-of-incidence-induced hysteresis was investigated both numerically and experimentally over a similar geometry. Based on the experimental findings of Ben-Dor *et al.*'s (2001) study, it is hypothesized that, in fact, four different wave configurations, three inviscid and one viscous, can be obtained for identical flow conditions. Since the geometry under investigation resembles supersonic intakes, this finding is relevant to their performance in supersonic/hypersonic flight.

---

## 1. Introduction

The reflection of oblique shock waves in steady flows (see e.g. Ben-Dor 1991, chap. 3) could result in two general types of wave configurations: a regular reflection (RR) and a Mach reflection (MR). Von Neumann (1945) suggested two extreme criteria for the RR ↔ MR transition, which were later termed the *detachment* and the *von Neumann criteria*. The two transition lines, arising from these two criteria, divide the  $(M_0, \phi_0)$ -plane, where  $M_0$  is the incident flow Mach number and  $\phi_0$  is the angle of incidence, into three different domains: a domain inside which only RR wave configurations are theoretically possible, a domain inside which only MR wave configurations are theoretically possible, and an intermediate domain, that is known as the *dual-solution domain*, inside which both RR and MR wave configurations are theoretically possible. The existence of a dual-solution domain led Hornung, Oertel & Sandeman (1979) to hypothesize that a hysteresis process could exist in the RR ↔ MR transition process. Chpoun *et al.* (1995) and Li, Chpoun & Ben-Dor (1999) recorded experimentally hysteresis processes in the reflection of two-dimensional symmetric and asymmetric shock waves, respectively. Fomin *et al.* (1996), Skews (1997, 1998) and Ivanov *et al.* (1998*a,b*) showed that the above-mentioned experimental results were contaminated by three-dimensional edge effects and therefore could not be considered as purely two-dimensional. Skews (2000) showed that three-dimensional edge effects are evident in wave configurations associated with the reflection of plane shock waves

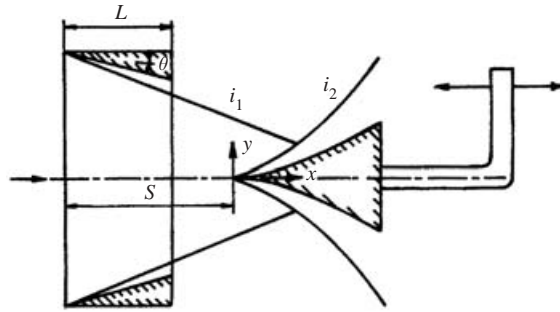


FIGURE 1. Schematic illustration of the geometrical set-up used in the present numerical study. An incident conical converging shock wave is generated using a conical ring with a sharp leading edge. This shock wave then interacts with a diverging conical curvilinear shock wave, which is generated by a curvilinear cone.

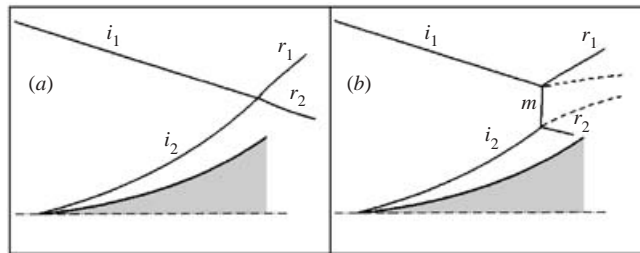


FIGURE 2. Schematic illustration of the two wave configurations, which were obtained in the present study. (a) An overall regular reflection (oRR) wave configuration. The wave configuration consists of an incident converging conical shock wave,  $i_1$ , generated by the conical ring, a head diverging conical shock wave,  $i_2$ , generated by the curvilinear cone, and two refracted shock waves,  $r_1$  and  $r_2$ . (b) An overall Mach reflection (oMR) wave configuration. The wave configuration consists of two Mach reflection wave configurations, which share a common Mach stem,  $m$ .

over plane wedges. The above studies regarding the three-dimensional effects raised doubts whether the hysteresis process is possible in two-dimensional flows. For this reason Ben-Dor *et al.* (2001) designed an experimental set-up aimed at answering the question of whether a hysteresis in the  $RR \leftrightarrow MR$  transition could exist in a flow field which is free of three-dimensional edge effects.

The geometrical set-up fulfilling this requirement is shown schematically in figure 1. An incident converging conical shock wave,  $i_1$  was generated using a conical ring with a sharp leading edge of angle,  $\theta$ . This incident converging conical shock wave interacted with a diverging curvilinear conical shock wave,  $i_2$ , which was generated by a curvilinear cone. Based on Ben-Dor *et al.*'s (2001) study, depending on the angle of interaction between these two conical shock waves, the resulting overall wave configuration could be either an overall regular reflection (oRR) or an overall Mach reflection (oMR). Schematic illustrations of both an oRR and an oMR wave configuration are shown in figures 2(a) and 2(b), respectively.

The angle of interaction between these two conical shock waves could, in principle, be altered either by (i) keeping the oncoming flow Mach number constant and changing the horizontal distance between the conical ring and the curvilinear cone or (ii) keeping the geometrical set-up fixed and changing the oncoming flow Mach number.

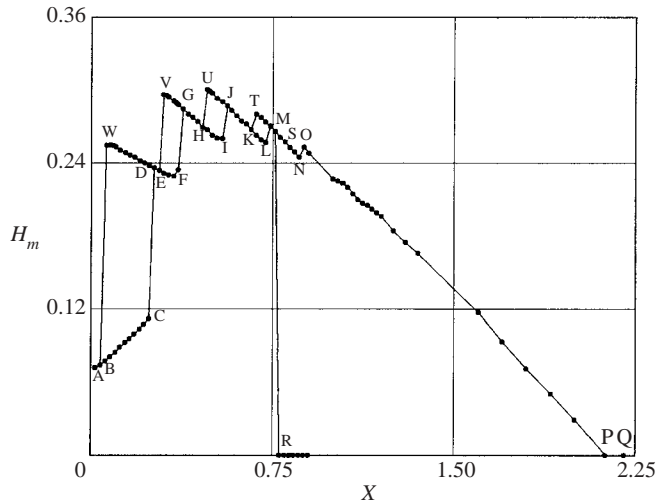


FIGURE 3. The numerically obtained angle-of-incidence-induced overall hysteresis loop. It consists of two types of hysteresis loops: one major one, SNOPRS, and four minor ones, BCDWB, EFGVE, HIJUH and KLMTK.  $H_m$  is the length of the Mach stem, i.e. the distance between the two triple points in the case of an oMR, and  $X = S/L$  is the non-dimensional distance of the nose of the curvilinear cone from the entrance cross-section of the conical ring ( $S$  and  $L$  are shown in figure 1).

Ben-Dor *et al.* (2001) investigated, both experimentally and numerically, option (i) of altering the angle of interaction between the two conical shock waves, namely changing the geometrical set-up while keeping the oncoming flow Mach number constant. By continuously moving the curvilinear cone along the axis of symmetry the angle of interaction between the two conical shock waves was altered and as a result both the oRR  $\rightarrow$  oMR and the oMR  $\rightarrow$  oRR transitions were observed and recorded. Ben-Dor *et al.* (2001) experimentally discovered a double-loop hysteresis consisting of one which was found to be viscous dependent, and another non-viscous dependent one which was associated with the existence of the previously-mentioned dual-solution domain. The experimental results clearly indicated that a hysteresis existed in a flow field that was free of three-dimensional edge effects. Not surprisingly, Ben-Dor *et al.* (2001) failed to detect the viscous-dependent hysteresis loop in their numerical Euler calculations, but did succeed in obtaining the non-viscous-dependent hysteresis loop. In addition, multiple minor hysteresis loops, associated with the interaction between the overall shock wave configuration and the rear edge (base) of the curvilinear cone, were also observed. While the non-viscous major hysteresis loop, which arose from the existence of a dual-solution domain, involved different overall wave configurations, i.e. oRR or oMR, the multiple minor hysteresis loops consisted of only oMR wave configurations with different flow patterns. The above-mentioned viscous-dependent hysteresis loop was obtained numerically by Burstchell *et al.* (2001) in their Navier–Stokes simulations.

The overall numerical hysteresis loop is shown in figure 3. Note that based on the experimental results of Ben-Dor *et al.* (2001) the viscous-dependent hysteresis loop overlapped the major hysteresis loop. Hence, it was indicated by Ben-Dor *et al.* (2001) that there were geometrical set-ups for which three different, two inviscid and one viscous, shock wave reflection configurations were possible.

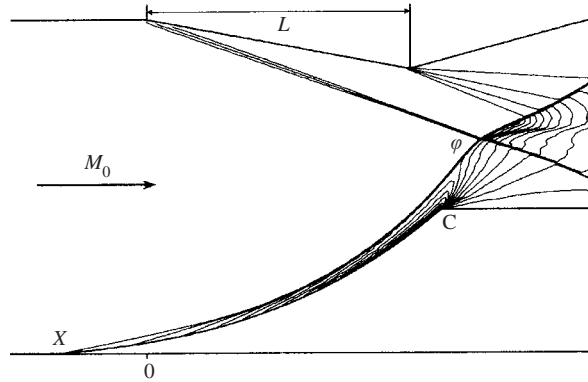


FIGURE 4. A typical wave configuration (isopycnics), which results from the interaction of a supersonic flow, having a flow Mach number  $M_0 = 5.5$ , with the investigated geometrical set-up. The principal feature of the developed flow is the formation of two conical shock waves: the *incident shock wave*, which is formed as a result of the interaction of the supersonic flow with the conical ring, and the *head shock wave*, which is formed as a result of the interaction of the supersonic flow with the curvilinear cone. The incident shock wave interacts with the head shock wave to give the overall wave configuration, which can be either an oRR (as shown in figure 2a and in this figure) or an oMR (as shown in figure 2b).

The option (ii) of altering the angle of interaction between the two conical shock waves, namely keeping the geometrical set-up fixed and changing the oncoming flow Mach number is the focus of the present study.

It should be noted here that while option (i) is relatively easy to investigate experimentally, it is very difficult to investigate experimentally option (ii), which is numerically investigated in the present study, since wind tunnels in which the flow Mach number can be altered in the test section, are not readily available. For this reason, while case (i) has been investigated both experimentally and numerically, the present case (ii) has been investigated only numerically. As the hysteresis processes are induced in different ways a new numerical code had to be written. In addition, it is important to note that since the geometry under investigation resembles supersonic intakes, the present investigation, as will be shown subsequently, is relevant to the performance of intakes at supersonic/hypersonic flights.

## 2. The geometrical set-up

The geometrical set-up that was used for the present investigation is shown in figure 1. It is identical to the one that was used by Ben-Dor *et al.* (2001). The choice of an identical geometrical set-up was made for convenience, i.e. it was already programmed. A 70 mm diameter and 28 mm wide conical ring was placed in a supersonic flow. The shape of the curvilinear cone was  $y(x) = 0.000115x^3 + 0.002717x^2 + 0.08749x$  ( $x$  and  $y$  are in mm). The base diameter and the length (height) of the curvilinear cone were 30.4 mm and 40 mm, respectively. The head angle of the conical ring was  $\theta = 10^\circ$ . The location of the curvilinear cone with respect to the conical ring was kept constant. The non-dimensional distance of the nose of the curvilinear cone from the entrance cross-section of the conical ring is defined as  $X = S/L$  where  $S$  and  $L$  are shown in figure 1,  $L$  being the width of the conical ring.

A typical calculation of the resulting flow field, for  $X = -0.3$  and  $M_0 = 5.5$ , is shown in figure 4. As mentioned earlier, the principal feature of the developed flow is the

formation of two conical shock waves. The one which is formed as a result of the interaction of the supersonic flow with the conical ring will be referred to as the *incident shock wave* and the other, which is formed as a result of the interaction of the supersonic flow with the curvilinear cone, will be referred to as the *head shock wave* of the cone. The incident shock wave interacts with the head shock wave in a manner that is known in the literature as a shock-on-shock interaction. Due to the curvature of the surface of the curvilinear cone the head shock wave is also curvilinear. However, owing to its interaction with the expansion fan emanating from the rear edge of the curvilinear cone (point C in figure 4), the head shock wave has an inflection point and it changes its curvature. The angle  $\varphi$  between the incident and the head shock waves depends on the location of the interaction point. If the interaction point is located downstream of the inflection point of the head shock wave (as is the case shown in figure 4) then the angle  $\varphi$  is small and the resulting overall wave configuration is an overall regular reflection (oRR). When the oncoming free-stream Mach number,  $M_0$ , is decreased the angle of the incidence of the shock wave increases, and the location of the intersection of the shock waves shifts upstream along the head shock wave. This, in turn, results in a considerable increase of the angle of interaction between the incident and the head shock waves, which could cause a transition to an overall Mach reflection (oMR).

### 3. The numerical method

The problem under consideration was solved using an Eulerian code for an ideal gas with  $\gamma = 1.4$ . The stationary solutions were determined numerically using a W-modification of the non-stationary Godunov method with second-order accuracy both in space and time. A detailed description of the W-modification of the non-stationary Godunov method can be found in Vasiliev (1996). General details of the code can be found in Ben-Dor *et al.* (1999).

The boundary conditions for these inviscid flows are straightforward. Because the free stream is supersonic the incoming flow conditions are specified, and the grid is chosen in such a way that the outgoing flow is also supersonic. Thus, a simple zeroth-order extrapolation of the variables at the outflow is appropriate. Along the cone and nozzle surfaces, both the normal velocity component and the normal pressure gradient are forced to be zero.

Godunov's method (as well as all the other methods which employ the solution of the Riemann problem) is very well suited to tracking shock wave fronts. Consequently, a procedure for tracking the Mach stem (if an oMR wave configuration was formed) was applied in the course of the present numerical calculations. This procedure transformed the mesh during the calculations in such a manner that part of one of the vertical boundary lines of the mesh coincided with the Mach stem. The remaining tracking lines were extended up to the boundaries of the channel as straight lines. As a result of tracking the Mach stem the vertical boundary lines of the mesh became curvilinear. The numerical details of the procedure for tracking the shock wave front, i.e. transformation of the numerical mesh in such a manner that part of one of the vertical boundary lines of the mesh would coincide with the Mach stem, are described in Vasiliev & Kraiko (1999).

The flow Mach number was varied continuously in the range  $2.6 \leq M_0 \leq 5.0$  with increment of  $\Delta M = 0.05$ . The procedure for varying the flow Mach number,  $M_0(t)$ , during the calculations for the same variant is shown by the left vertical axis of figure 5. The overall time for varying the flow Mach number was composed of

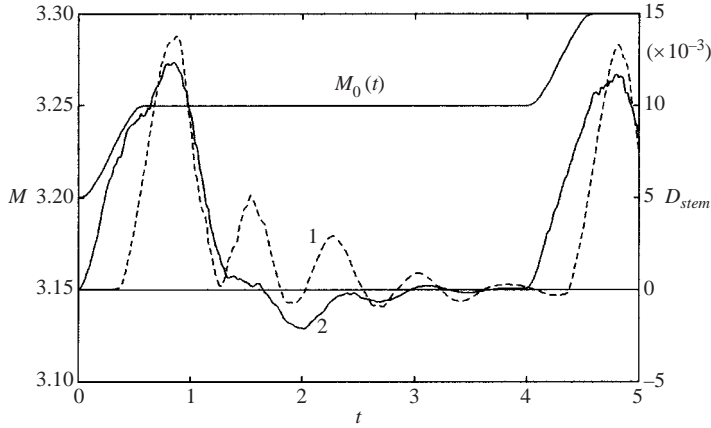


FIGURE 5. The procedure of varying the flow Mach number  $M_0(t)$  during the calculations.  $D_{stem}$  (dashed line) is the non-dimensional velocity of the middle point of the Mach stem. Curve 2 is the result using equations (2).

two intervals: a transitional time,  $\Delta t_{trans}$ , and an interval,  $\Delta t_{total}$ , which was the time taken for the stationary solution to reach a situation for which  $M_0(t) = \text{const}$ . The values of these time intervals were established, based on our preliminary calculations, respectively, as

$$\Delta t_{trans} = 0.6 \frac{L}{a_0}, \quad \Delta t_{total} = 4 \frac{L}{a_0}. \quad (1)$$

In (1)  $a_0$  is the speed of sound of the free stream. (Note that in figure 5 and in the following the dimensionless time  $L/a_0$ , is used). The main criterion for determining whether a stationary solution has been reached was the stabilization of the Mach stem (in the cases when the resulting wave configuration was an oMR). It was assumed that a stationary solution was reached if the non-dimensional velocity of the middle point of the Mach stem,  $D_{stem}$ , fulfilled, during a pre-determined time interval, the condition  $D_{stem} = V_{stem}/a_0 \leq 0.0002$ , where  $V_{stem}$  is the velocity of the middle point of the Mach stem. (Note that in the following the dimensionless velocity (non-dimensionalized by  $a_0$ ) is used.) If at the end of the overall time interval allocated for the stationary solution to be reached, the above-mentioned condition was not satisfied the calculations were allowed to continue. The overall time interval allocated in the calculations with an oRR was sufficient to within a factor of 0.5.

The main role of a transitional time interval with a smooth  $M_0(t)$  is to prevent large transient disturbances in the flow field from delaying the steady flow formation or provoking an untimely transition from one wave configuration to another. For the same purpose, i.e. for the suppression of the transient disturbances, it is possible to use a change of parameters not only in time, but also in space. For example to change  $M_0(t)$  it is possible to:

- (a) change the flow parameters only at the inflow face;
- (b) change the flow parameters in the entire uniform flow ahead of the shock waves;
- (c) modify the non-uniform flow behind the shock waves.

It is clear that case (a) is not optimal, since it includes a time delay which is needed for the changes of the parameters to reach the position of the shock waves.

The dashed line in figure 5 represents the time variation of the dimensionless velocity of the front of the Mach stem,  $D_{stem}$ , when the generation of the changes takes place at the inflow face, i.e. case (a). One can see that the time delay in the response of the front of the Mach stem to the changes in the incident flow is approximately 0.4. The oscillatory nature of the damping of the front velocity of the Mach stem, and therefore of all the flow properties, can also be seen in figure 5. Note that the required criterion for reaching a stationary condition  $D_{stem} \leq 0.0002$  by  $t = 4$  was not met in the case shown in figure 5.

An adaptive mesh of  $360 \times 180$  was employed in the calculations. The mesh was refined in the region where the interaction took place and in the direction of the rear edge of the cone (point C in figure 4). All the other details of the numerical procedure are identical to those used in our previous study (Ben-Dor *et al.* 2001).

The correction of the parameters of the flow field at the transient stage of the variation of the flow Mach number was performed using the Rankine–Hugoniot relations for strong shock waves (with  $\lambda = 1$ ) but implemented with  $\lambda = 0.5$ :

$$\left. \begin{aligned} p(t + \tau) &= p(t) + 2\lambda(p(t) - p_0) \frac{M(t + \tau) - M(t)}{M(t)}, \\ \rho(t + \tau) &= \rho(t) + \lambda(\rho(t) - \rho_0)^2 \frac{(\gamma + 1) M(t + \tau) - M(t)}{\rho_0 M^2 M(t)}, \\ q(t + \tau) &= q(t) \frac{\rho(t)}{\rho(t + \tau)} \frac{M(t + \tau)}{M(t)}, \end{aligned} \right\} \quad (2)$$

where  $\tau$  is the magnitude of the time step. This procedure allowed us to change only the upstream velocity and keep the density and the pressure constant. The efficiency of this approach is demonstrated in figure 5 where the solid lines show the results obtained using equations (2). In this case the maximum of the velocity amplitude is lower, but the main advantage is that the damping of the oscillations after a transient stage (when equations (2) are not yet applied) occurs faster. Here the criterion for attaining a stationary flow was achieved at a time equal to 3.8. The application of this procedure enabled us to reduce the computational time at the transient stage by 25–30%. If at the end of a stabilization interval the criterion was not satisfied, only this case needed to be calculated further since prior to the beginning of each transient stage all the parameters of the flow field were stored in a separate file.

#### 4. The numerical results

Three cases were investigated in the present numerical study. They differed in the location of the curvilinear cone with respect to the conical ring, i.e. in the value of  $X$ . The three values of  $X$  that were investigated were  $-0.3$ ,  $-0.2$  and  $-0.1$ . (The minus sign means that the nose of the curvilinear cone was located upstream of the entrance cross-section of the conical ring as is shown in figure 4 where 0 indicates the location of the entrance cross-section of the conical ring). The numerical results of these three simulations are presented in the following.

##### 4.1. Case 1: $X = -0.3$

The dependence of the Mach stem length,  $H_m$ , i.e. the distance between the two triple points of an oMR, on the free-stream flow Mach number,  $M_0$ , when the latter was changed from  $4.8 \rightarrow 2.6 \rightarrow 4.8$  is shown in figure 6. Note that  $H_m = 0$  when the resulting wave configuration is an oRR.

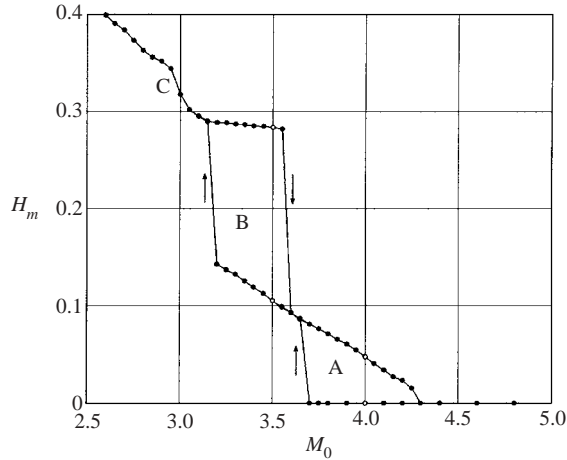


FIGURE 6. The dependence of the Mach stem length on the free-stream-flow Mach number when it was changed from  $4.8 \rightarrow 2.6 \rightarrow 4.8$  for  $X = -0.3$ . The two wave configurations of loop A that are appropriate to  $M_0 = 4$  are shown in figures 7(a) and 7(b), and the two wave configurations of loop B that are appropriate to  $M_0 = 3.5$  are shown in figures 7(c) and 7(d).

As is evident in figure 6, an oRR interaction between the two shock waves takes place during the variation of the flow Mach number from 4.8 to 3.8. A sudden transition from an oRR to an oMR occurs at  $M_0 = 3.65$ . Further reduction of  $M_0$  is associated with a gradual increase in the length of the Mach stem. This trend continues until  $M_0 = 3.15$  where a sudden sharp increase of the Mach stem length is observed. This transition is caused by the intersection of the reflected shock wave of the lower Mach reflection with the rear edge of the curvilinear cone. Had the curvilinear cone had a different geometry this transition would have most likely taken place at a different value of  $M_0$ . When the direction of changing the flow Mach number is reversed and it is increased the reversed transitions occur at different values of  $M_0$ . Consequently, two hysteresis loops, A and B, are observed. While loop A involves both oRR and oMR wave configurations, loop B involves only oMR wave configurations, which are associated with different lengths of the Mach stems and, as a result, different overall flow patterns.

The wave configurations associated with the hysteresis loops A and B are shown in figures 7(a,b) and 7(c,d), respectively. The computer-generated frames illustrate constant density contours, i.e. isopicnics, for the flow Mach numbers,  $M_0 = 4.0$  and 3.5. These wave configurations correspond to the open circles along the hysteresis loop in figure 6. The important role of the rear edge of the curvilinear cone (point C in figure 4) in the formation of the hysteresis loop B is clearly seen in figure 7(c,d). It is hypothesized here that had the curvilinear cone had a different shape a multiplicity of hysteresis loops would still be obtained but at different values of the flow Mach number. (A further discussion regarding this matter appears in the conclusions.)

Note, in figure 6, the sudden increase in the length of the Mach stem when the reflected shock wave of the lower Mach reflection reaches the rear edge of the curvilinear cone, as the flow Mach number is reduced from 3.2 to 3.1. Had the curvilinear cone had a different geometry this transition would have taken place at a different value of  $M_0$ . It is also interesting to note that loop B is very similar to one of the hysteresis loops which were numerically discovered in our previous study (see figure 8 in Ben-Dor *et al.* 2001).

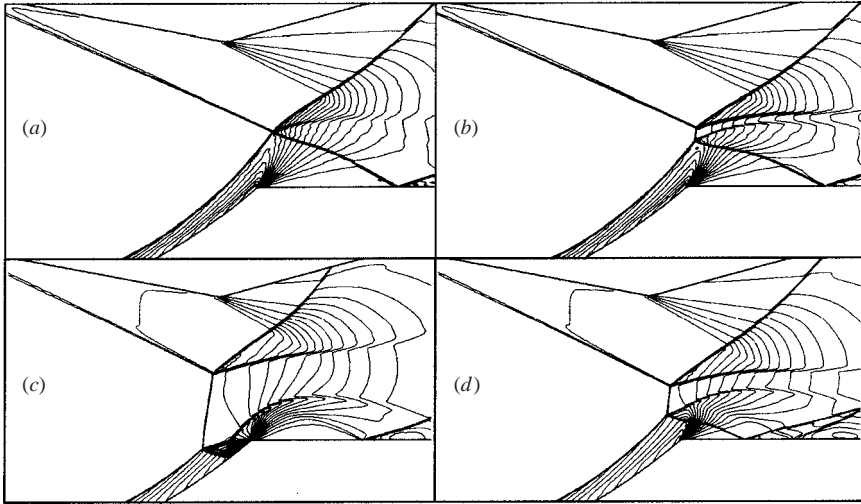


FIGURE 7. The dual wave configurations associated with the hysteresis loop A for  $M_0 = 4.0$ , (a) and (b), and the hysteresis loop B  $M_0 = 3.5$ , (c) and (d) of figure 6.

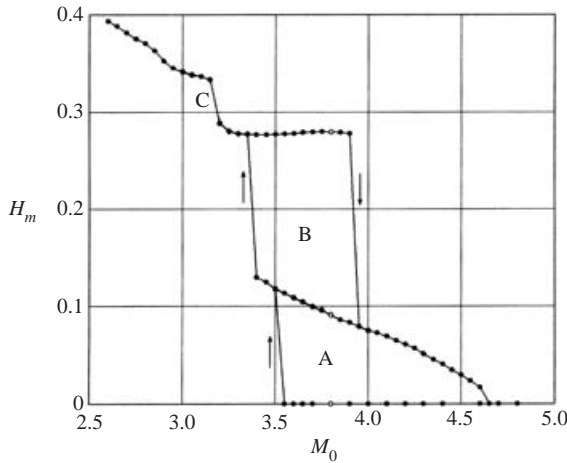


FIGURE 8. The dependence of the Mach stem length on the free-stream-flow Mach number when it was changed from  $4.8 \rightarrow 2.6 \rightarrow 4.8$  for  $X = -0.2$ . The three wave configurations of loops A and B that are appropriate to  $M_0 = 3.8$  are shown in figures 9(a), 9(b) and 9(c).

4.2. Case 2:  $X = -0.2$

Similar calculations to those presented for case 1 are presented for this case in figures 8 and 9. In this case the curvilinear cone was located slightly downstream of its location in case 1. The dependence of the Mach stem length on the free-stream-flow Mach number when the latter was changed from  $4.8 \rightarrow 2.6 \rightarrow 4.8$  is shown in figure 8. It is evident from figure 8 that the change in the location of the curvilinear cone resulted in a significant increase of the range of the hysteresis loop A. As a result, unlike the previous case, now the hysteresis loops A and B overlap. This in turn results in a situation in which there is a flow Mach number range for which three stationary

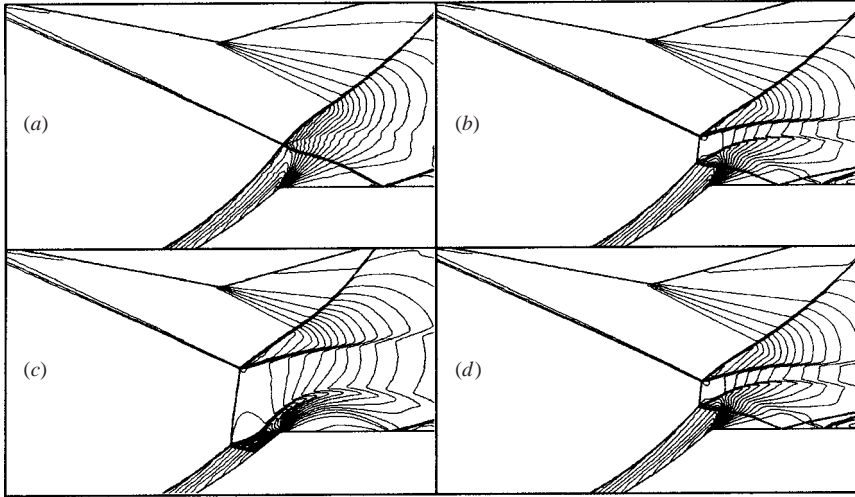


FIGURE 9. Three different wave configurations at  $M_0 = 3.8$  associated with the hysteresis loop A, (a) and (b), and the hysteresis loop B, (c) and (d), of figure 8.

wave configurations, one oRR and two oMRs, are possible. Three such different wave configurations, for  $M_0 = 3.8$ , are shown in figure 9, in which the wave configurations (a,b) and (c,d) that are associated with the hysteresis loops A and B are presented, respectively. These wave configurations correspond to the open circles in figure 8. The important role of the rear edge of the curvilinear cone (point C in figure 4) in the formation of the hysteresis loop B is again clearly seen in figure 9.

It should be noted here that these three possible wave configurations are all derived from the solution of the Euler equations. Hence, they are all inviscid. Recalling that Ben-Dor *et al.* (2001) also obtained experimentally a viscous wave configuration, which is also possible for the geometrical configuration that is investigated here, means that a unique situation in which four different wave configurations, three inviscid and one viscous, are, in fact, possible for the same flow conditions. To the best of our knowledge, a situation in which four different wave configurations are possible for the same flow conditions has never been reported before.

#### 4.3. The pressure distributions for cases 1 and 2.

As mentioned earlier, the hysteresis loop B (see figure 8) involves two different oMR wave configurations, one having a longer Mach stem than the other. The pressure distributions along the curvilinear cone for these two different oMRs, for  $M_0 = 3.5$ , are shown in figure 10(a). The respective wave configurations are shown in figures 7(c) and 7(d). It is clearly evident from figure 10(a) that the different oMR wave configurations are associated with pressure distributions which significantly differ from each other. While the pressure profile associated with the oMR having the shorter Mach stem is seen to gradually increase to a value about 10 times larger than the ambient pressure, the pressure profile associated with the oMR having the longer Mach stem has a pressure peak which is more than 40 times larger than the ambient pressure. An inspection of the corresponding wave configurations in figure 7(c,d) clearly explains this difference. The Mach stem of the oMR having the longer Mach stem is positioned further upstream than that having the shorter Mach stem. As a result the reflected shock wave of the lower Mach reflection hits the cone surface and reflects from it as

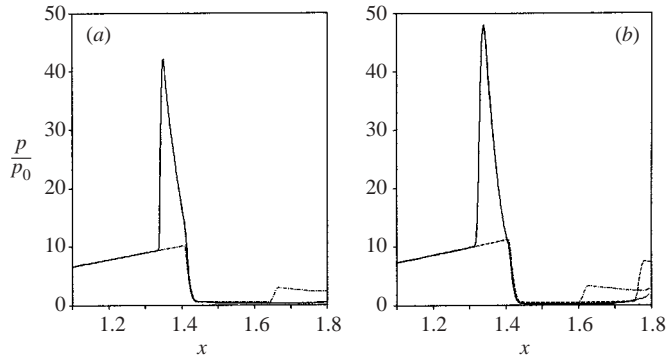


FIGURE 10. The pressure distribution along the cone surface for (a)  $M_0 = 3.5$  (loop B of figure 8), and (b) for  $M_0 = 3.7$  (loops A and B of figure 8). The distance is measured from the nose of the cone. Solid line – oMR wave configuration having a long Mach stem; dash-dotted line – oMR wave configuration having a short Mach stem; dashed line – oRR wave configuration.

a regular reflection, RR. This RR is the reason for the pressure peak that is seen in figure 10(a).

Owing to the absence of this RR in the oMR wave configurations of the hysteresis loop A (see figure 7(a,b)) no visible difference was found in the pressure distributions of the oRR and the oMR wave configurations associated with this hysteresis loop.

The pressure distributions along the curvilinear cone for  $M_0 = 3.7$  for which the hysteresis loops A and B overlap and hence three wave configurations (an oRR, an oMR with a short Mach stem and an oMR with a long Mach stem) are possible, are shown in figure 10(b). While the pressure distributions for the cases of the oRR and the oMR having the short Mach stem (see figure 9a,b) are quite similar, both are seen to gradually increase to a value slightly larger than 10 times the ambient pressure, the pressure distribution for the oMR having the longer Mach stem (see figure 9c) is again seen to have a sharp peak which reaches a value that is almost 50 times larger than the ambient pressure. The reason is again the reflection of the reflected shock wave of the lower Mach reflection from the cone surface for the case of an oMR having a long Mach stem.

#### 4.4. Case 3: $X = -0.1$

The results of the numerical calculation are shown in figures 11 to 13. In this case the curvilinear cone is located slightly downstream of its location in case 2. The dependence of the Mach stem length on the free-stream-flow Mach number when the latter was changed from  $5.0 \rightarrow 2.6 \rightarrow 5.0$  is shown in figure 11.

It is evident from figure 11 that the change in the location of the curvilinear cone resulted in a further significant increase of the range of the hysteresis loop A. Furthermore, unlike the previous two cases, now there are three hysteresis loops: the previously obtained loops A and B and a small additional loop, loop C. During the calculation of this hysteresis loop the increment of the Mach number  $\Delta M_0$  was reduced by a factor 2, i.e.  $\Delta M_0 = 0.025$ . Similarly to the previous case here again the hysteresis loops overlap. There is an overlap of loops A and C, and an overlap of loops A and B. Consequently, once again based on the inviscid numerical simulation, three different wave configurations for identical flow conditions (flow Mach number and geometry), are possible. The wave configurations associated with the hysteresis loop A are shown in figure 12 and the wave configurations that correspond to the

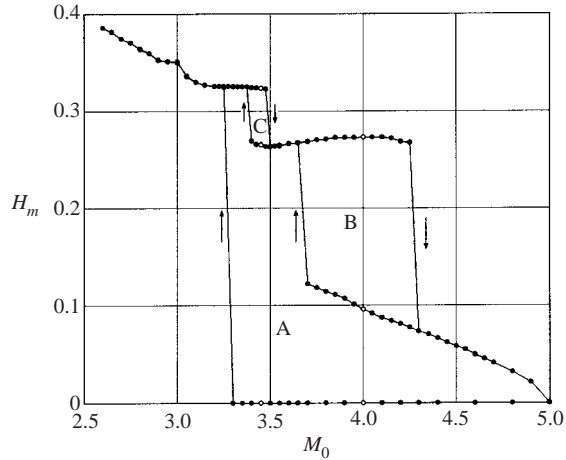


FIGURE 11. The dependence of the Mach stem length on the free-stream-flow Mach number when it was changed from  $5.0 \rightarrow 2.6 \rightarrow 5.0$  for  $X = -0.1$ . The two wave configurations of loop A that are appropriate to  $M_0 = 4$  are shown in figures 12(b) and 12(d), and the two wave configurations of loop C that are appropriate to  $M_0 = 3.45$  are shown in figures 13(c) and 13(d).

hysteresis loops B and C are shown in figure 13. The important role of the rear edge of the curvilinear cone in the formation of the hysteresis loops B and C is clearly seen, once again, in figure 12.

The earlier note regarding the possible existence of a fourth, viscous dominated, wave configuration for the same flow conditions, holds also in this case.

Figures 14(a) and 14(b) represent the pressure distributions for  $M_0 = 3.45$  for which loops A and C overlap, and  $M_0 = 4.0$ , for which loops A and B overlap. Three different wave configurations – an oRR, an oMR having a short Mach stem and an oMR having a longer Mach stem – are possible for each of these two flow Mach numbers (see the open circles in figure 11). Unlike the previous cases, now the pressure distribution associated with the oMR having the longer Mach stem has two pressure peaks. While the first peak is about 37 times higher than the ambient pressure the second peak is about 24 times higher than the ambient pressure. The reason for the double-peak pressure profile is clearly understood when the actual wave configuration, that is shown in figure 13(c), is examined. The first peak is due to the reflection of the reflected shock wave of the lower Mach reflection from the cone surface, which unlike in the previous case now reflects as a Mach reflection, MR, rather than as a regular reflection, RR. The second peak arises from the strong compression near the shoulder of the curvilinear cone, where a hump in the contact discontinuity is seen to develop over the cone surface. The pressure enhancement at the edges of such a hump has been addressed in our previous study (Ben-Dor *et al.* 2001).

The pressure distribution associated with the oRR is again seen to gradually increase to a value that is about 10 times larger than the ambient pressure. Unlike the previous cases (see figure 10) where the pressure distributions of the oMR having the shorter Mach stem were seen to gradually increase to values of about 10 times higher than the ambient pressure, now the pressure distribution of the oMR having the shorter Mach stem also has a pressure peak which is almost 40 times the ambient pressure. The reason for this behaviour is self-explanatory in view of the forgoing

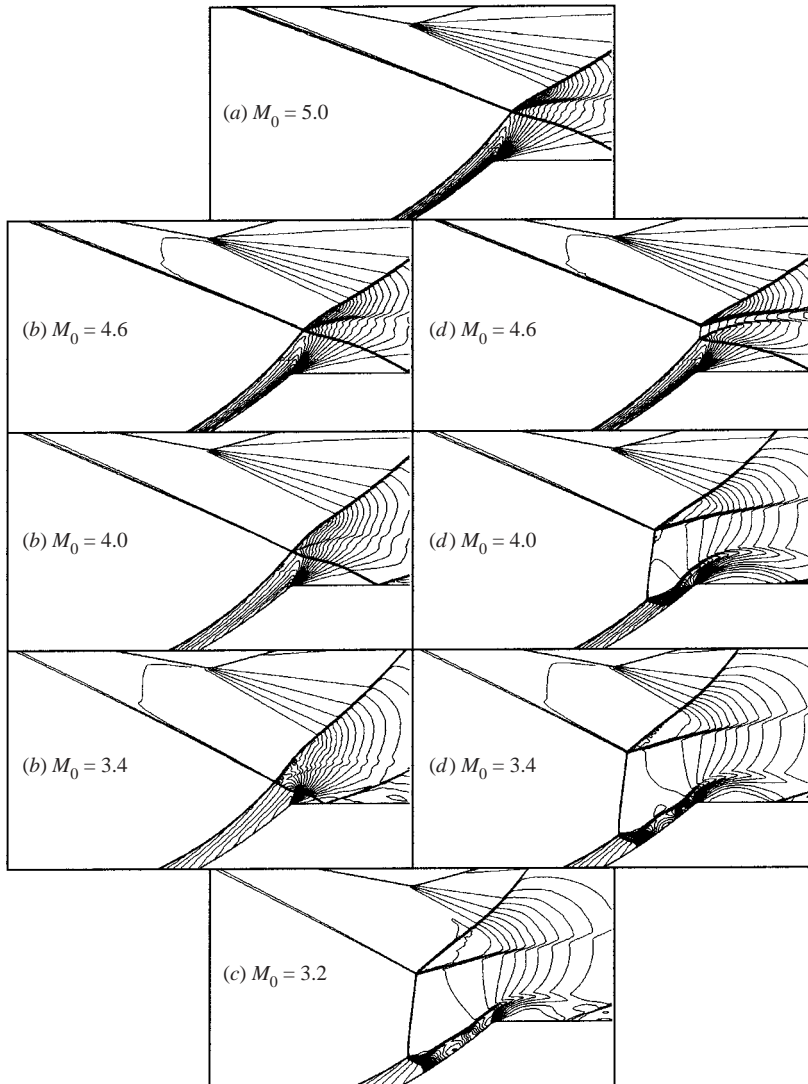


FIGURE 12. The wave configurations of the hysteresis loop A ( $a \rightarrow b \rightarrow c \rightarrow d \rightarrow a$ ) of figure 11.

explanations and an inspection of the actual wave configuration that is shown in figure 13(*d*.)

At  $M_0 = 4.0$  (see figure 14*b*) pressure distributions similar to those shown in figure 10 are again obtained. While the pressure distribution for the oMR having the longer Mach stem has a pressure peak which is more than 48 times larger than the ambient pressure, the pressure distributions of both the oMR having the shorter Mach stem and the oRR are again seen to be very similar. They both gradually increase to values slightly larger than 12 times the ambient pressure.

It is evident from the foregoing presentation and discussion regarding the pressure distributions associated with the various wave configurations (see figures 10 and 14) that the pressure distributions of oMR wave configurations having Mach stems which are about  $0.3L$  long ( $L$  is the width of the conical ring) are associated with pressure

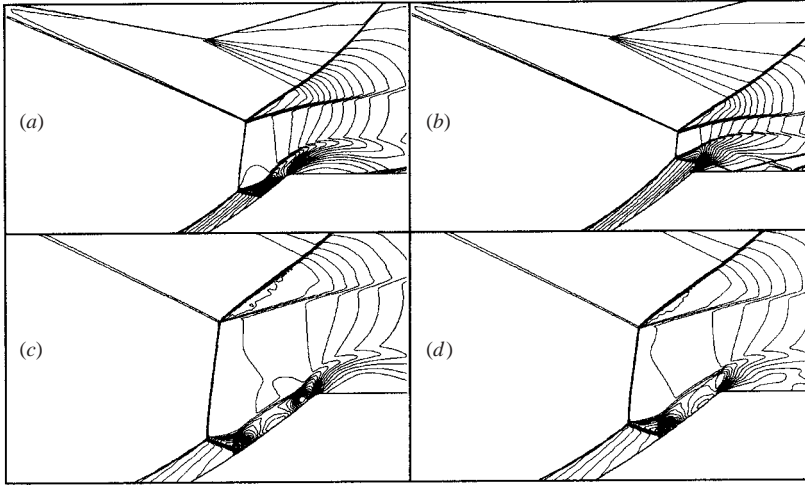


FIGURE 13. The dual wave configurations associated with the hysteresis loop B,  $M_0 = 3.95$ , (a) and (b), and the hysteresis loop C,  $M_0 = 3.45$ , (c) and (d), of figure 11.

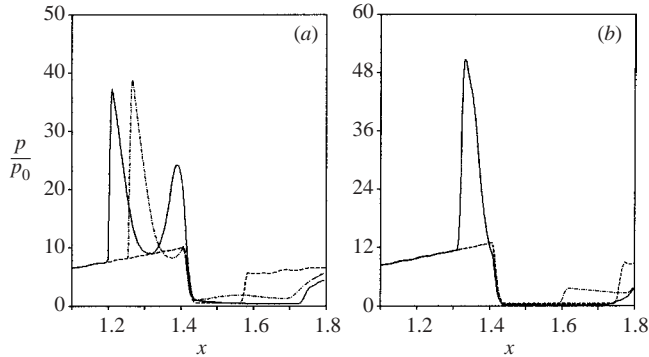


FIGURE 14. The pressure distribution along the cone surface for (a) the wave configurations of loops A and C,  $M_0 = 3.45$ , and (b) loops A and B,  $M_0 = 4.0$ , of figure 11. Solid line – oMR configuration with a long Mach stem; dash-dotted line – oMR configuration with a short Mach stem; dashed line – oRR configuration.

peaks which are about 40–50 times larger than the ambient pressure. In the case of oMR wave configurations having Mach stems which are only about  $0.1L$  long, the pressure distributions are similar to those of oRR wave configurations. The reason for the difference in the pressure distributions is the fact that the Mach stem of the oMR wave configurations having long Mach stems are positioned further upstream than the Mach stem of the oMR wave configurations having short Mach stems. As a result the reflected shock waves of the lower Mach reflections of the oMR wave configurations reflect from the surface of the curvilinear cone, either as an RR or an MR. This in turn results in the pressure peaks. The pressure peak is higher when the reflection is an RR.

## 5. General remarks

The numerical simulations of cases 2 and 3 presented above, which resulted in different stationary solutions for identical flow conditions, must be accounted for

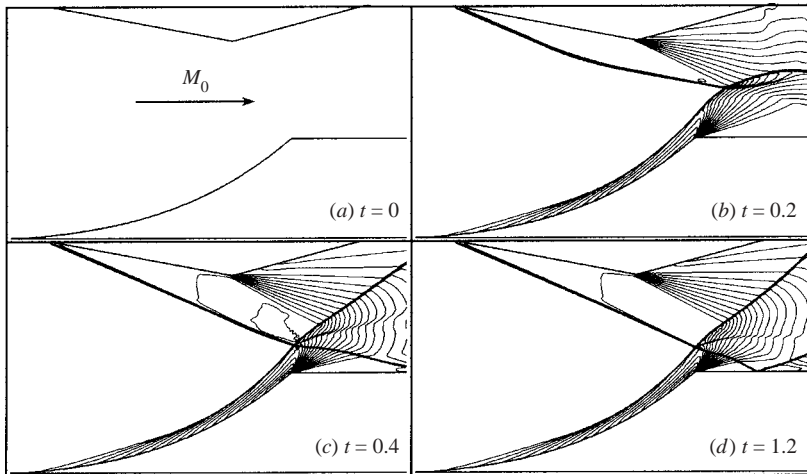


FIGURE 15. The evolution of a stationary flow with a uniform flow with Mach number  $M_0 = 4.0$  as the initial condition for the calculations.

when conducting numerical simulations, as the lack of information about these solutions could lead to paradoxes.

The evolution of a stationary flow for an identical flow Mach number,  $M_0 = 4.0$ , but three different ways of initializing the numerical code, is shown in figures 15 and 16. A uniform flow with a Mach number  $M_0 = 4.0$ , was the initial condition for the calculations shown in figure 15. A normal discontinuity of pressure and velocity, which induces behind it a uniform supersonic flow with a flow Mach number,  $M_0 = 4.0$ , was the initial condition for the calculations shown in figure 16. The difference between the two sequences shown in figure 16 is the initial pressure,  $p_1$ , of the quiescent gas downstream of the front of the discontinuity. As can be seen in figures 15 and 16 the three calculations result in different stationary solutions, that represent the three possible wave configurations mentioned earlier, namely an oRR (in figure 15), and two oMRs, one with a long Mach stem and the other with a short Mach stem (in figure 16). While a multiplicity of solutions for a straight cone or for a wedge are predicted theoretically for a regular/irregular interaction, the multiplicity of solutions with different oMR wave configurations is, to the best of the authors' knowledge, not explained by any known theory.

## 6. Possible applications

It is important to note here that in spite of the fact that our motivation in studying the hysteresis process in the  $RR \leftrightarrow MR$  transition was purely academic, it turned out recently that the existence of the hysteresis processes might have an important impact on the performance of air intakes in supersonic and hypersonic flights. Consequently, there is a clear aeronautical and aerospace engineering interest in better understanding the hysteresis phenomenon investigated here.

Since the geometry investigated resembles the geometry of supersonic intakes, the findings regarding the existence of hysteresis processes, in general, and overlapping hysteresis processes, in particular, presented earlier can be relevant to the performances of the air intakes of vehicles flying at supersonic and hypersonic speeds. It should be noted here that by the term 'resemble' we mean that actual air intakes have geometries

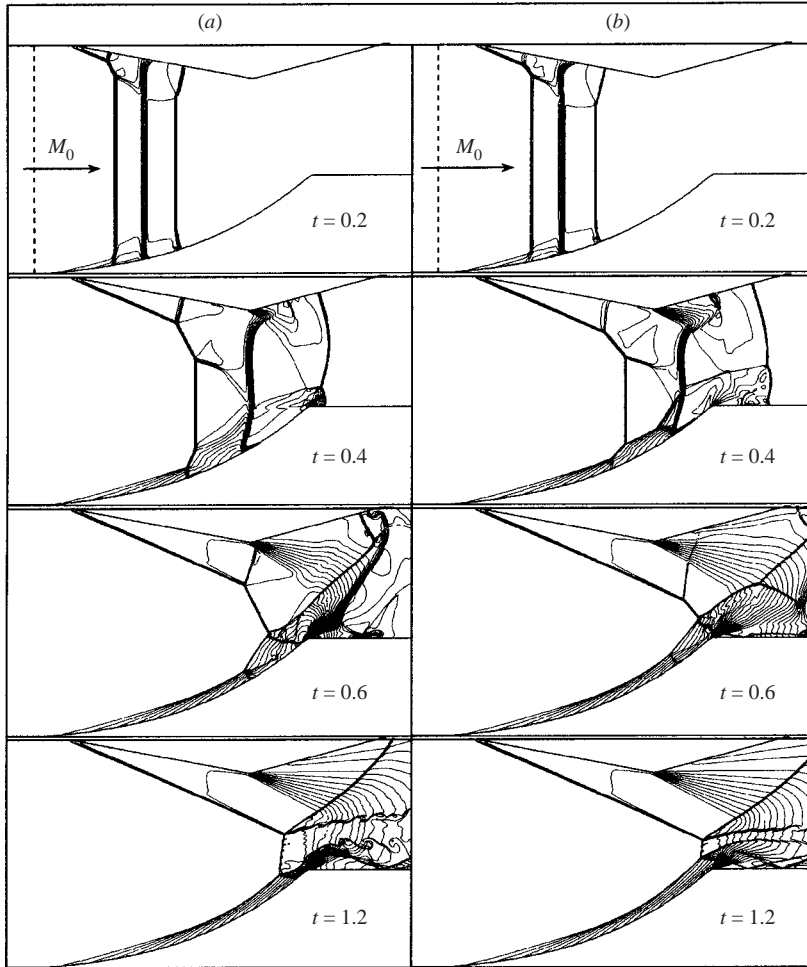


FIGURE 16. The evolution of a stationary flow with a normal shock wave, which induces behind it a uniform flow with Mach number  $M_0 = 4.0$  as the initial condition for the calculations. (a)  $p_0/p_1 = 5$ , and (b)  $p_0/p_1 = 10$ .

involving concave and convex axi-symmetric cylindrical and conical surfaces, which in supersonic flight would generate curvilinear shock waves. The angle of interaction of these curvilinear shock waves, which depends on the flight Mach number, might change in a range that will result in a hysteresis of the flow field associated with the air intake. This was pointed out by Onofri & Nasuti (2001) who were the first to relate the hysteresis phenomenon in the RR  $\leftrightarrow$  MR transition to the performance of air intakes. However, their numerical study was performed using a two-dimensional geometry, which resembles actual supersonic air intakes less than our axisymmetric geometry.

The possible dependence of the flow pattern, in general, and the pressure distribution, in particular, inside an air intake on the preceding variations in the speed of flight of a supersonic/hypersonic aircraft should be accounted for in the designing of intakes and flight conditions for supersonic and hypersonic vehicles. This is especially due to the fact that different flow fields would result in different

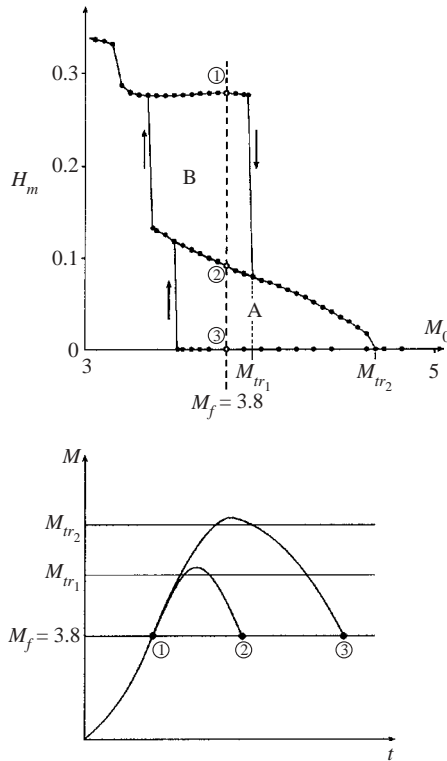


FIGURE 17. Schematic illustration of the possibility of obtaining three different wave configurations ((1) an oMR with a long Mach stem, (2) an oMR with a short Mach stem and (3) an oRR) inside a supersonic intake at the same flight Mach number,  $M_f = 3.8$ . The different wave configurations yield different flow fields which in turn could influence the entire performance.

flow conditions that can significantly affect the combustion processes and the overall performances of the vehicle.

Consider figure 17, the upper part of which is a reproduction of figure 8. The overlap of the hysteresis loops A and B suggests, as mentioned earlier, that there is a flow Mach number range for which three different wave configurations are possible. For example for the flight Mach number  $M_f = 3.8$  one can obtain an oMR wave configuration with a long Mach stem, or an oMR wave configuration with a short Mach stem, or an oRR wave configuration. These three wave configurations that are shown in figure 9 are marked in figure 17 as (1), (2) and (3), respectively. The flow Mach numbers at which the transitions from an oMR wave configuration with a long Mach stem to an oMR wave configuration with a short Mach stem and from an oMR wave configuration with a short Mach stem to an oRR wave configuration take place are labelled  $M_{ir1}$  and  $M_{ir2}$ , respectively. The lower part of figure 17 shows possible flight Mach number histories of a supersonic vehicle whose air intake is identical in geometry to that shown in figure 1 and the leading edge of the curvilinear cone is located at  $X = -0.2$ . At  $t = 0$  the vehicle starts accelerating to reach a flight Mach number of  $M_f = 3.8$ . Having reached this speed the wave configuration in its supersonic intake will be an oMR wave configuration with a long Mach stem (figure 9c). If at this stage the vehicle accelerates to a speed in the range  $M_{ir1} < M_f < M_{ir2}$  and then returns to  $M_f = 3.8$  then the wave configuration in the

supersonic air intake will change to an oMR with a short Mach stem (figure 9d). If, however, the vehicle accelerates to a speed in the range  $M_f > M_{tr_2}$  and then returns to  $M_f = 3.8$ , then the wave configuration in the supersonic air intake will change to an oRR (figure 9a). Consequently, as shown in this example, three different wave configurations might be encountered in the supersonic intake for identical supersonic flight speeds, i.e.  $M_f = 3.8$ . As shown earlier, these different wave configurations are associated with different pressure distributions and hence different dynamic and thermodynamic properties. The different flow fields would result in different flow conditions that could significantly affect the combustion process inside the air intake and the overall performance of the vehicle.

It should be noted here once again that these three possible wave configurations are all derived from the solution of the Euler equations. Hence, they are all inviscid. Recalling that Ben-Dor *et al.* (2001) also obtained experimentally a viscous-dependent wave configuration, which is also possible for the geometrical configuration investigated here, results in a unique situation in which four different wave configurations are, in fact, possible for the same flow conditions.

Finally, it should be mentioned that the present physical model is limited to perfect gas behaviour. However, at supersonic/hypersonic flights non-stationary and real gas effects, inside the air intakes, will most probably affect the resulting flow field. Consequently, the question of whether hysteresis processes will occur in actual cases is yet to be answered by simulating geometries of actual air intakes and accounting for both viscous and real gas effects. The findings of the present investigation clearly indicate that there is a possibility of hysteresis processes inside actual air intakes and that this should be accounted for when designing air intakes for supersonic/hypersonic flights.

## 7. Conclusions

A flow-Mach-number-induced hysteresis phenomenon, in the shock-on-shock interaction of conical shock waves was investigated numerically using a W-modification of the non-stationary Godunov method with second-order accuracy both in space and time. The interaction resulted in a multiplicity of hysteresis loops. The range of the hysteresis loops was found to depend on the location of the nose of the curvilinear cone with respect to the conical ring. Furthermore, it was found that for certain locations there were flow Mach number ranges in which three different inviscid wave configurations could be obtained for identical flow conditions. Since an additional viscous-dependent wave configuration is also possible for the investigated phenomenon, it can be concluded that there are flow Mach number ranges in which four different wave configurations, three inviscid and one viscous, can be obtained for identical flow conditions. As already mentioned to the best of our knowledge, a situation in which four different wave configurations are possible for the same flow conditions has never been reported before.

The different wave configurations for identical flow Mach numbers were associated with different pressure distributions. In cases where the Mach stem of the oMR wave configuration was long enough, pressure peaks that exceeded the ambient pressure by 40–50 times were obtained.

It is important to note here that the specific geometry of the curvilinear cone that was investigated in the course of this study was chosen in order to promote the RR ↔ MR transition. Consequently, the overall hysteresis loops for the three cases investigated, i.e. those shown in figures 6, 8 and 11, are specific to the chosen geometry

and not general. However, it is hypothesized here that the above described complicated hysteresis processes could be also encountered in other cases of supersonic flows over similar geometries, which will also generate interacting conical shock waves. Such geometries are those of air intakes of supersonic vehicles. It goes without saying that the flow Mach numbers at which transitions between the various wave configurations will occur for other geometries will be different from those found in the course of this study. The importance of the present study lies in the fact that it identifies a phenomenon in which up to four different steady flow fields could be established for identical flow conditions. In addition, in view of the fact that many similar flows are actually non-stationary, it is possible that the above-described situation of multiplicity of solutions is even more complex.

Since the geometry investigated resembles the geometry of supersonic air intakes, the findings regarding the hysteresis processes that are reported in the present study can be relevant to the flight performance at high supersonic speeds. The possible dependence of the flow pattern, in general, and the pressure distribution, in particular, inside the air intake on the preceding manoeuvres of an aircraft should be taken into account in the designing of air intakes and flight conditions for hypersonic vehicles.

This study complements an earlier study by Ben-Dor *et al.* (2001) in which an angle-of-incidence-induced hysteresis was investigated both numerically and experimentally over a similar geometry.

This study was conducted under the auspices of the Dr Morton and Toby Mower Professorial Chair of Shock Wave Studies.

#### REFERENCES

- BEN-DOR, G. 1991 *Shock Wave Reflection Phenomena*. Springer.
- BEN-DOR, G., ELPERIN, T., LI, H. & VASILIEV, E. I. 1999 The influence of downstream-pressure on the shock wave reflection phenomenon in steady flows. *J. Fluid. Mech.* **386**, 213–232.
- BEN-DOR, G., VASILIEV, E. I., ELPERIN, T. & CHPOUN, A. 2001 Hysteresis phenomena in the interaction process of conical shock waves: experimental and numerical investigations. *J. Fluid. Mech.* **448**, 147–174.
- BURSTCHELL, Y., ZEITOUN, D., CHPOUN, A. & BEN-DOR, G. 2001 Conical shock interactions in steady flows: Numerical study. *Proc. 23rd Intl Symp. on Shock Waves, Fort Worth TX, USA* (ed. F. K. Lu).
- CHPOUN, A., PASSEREL, D., LI, H. & BEN-DOR, G. 1995 Reconsideration of oblique shock wave reflection in steady flows. Part 1. Experimental investigation. *J. Fluid. Mech.* **301**, 19–35.
- FOMIN, V. M., HORNUNG, H. G., IVANOV, M. S., KHARITONOV, A. M. & KLEMENKOV, G. P. 1996 The study of transition between regular and Mach reflection of shock waves in different wind tunnels. *Book of Abstracts, 12th Intl Mach Reflection Symp., University of Wilwatersrand, Johannesburg, South Africa* (ed. B. W. Skews).
- HORNUNG, H. G., OERTEL, H. & SANDEMAN, R. J. 1979 Transition to Mach reflection of shock waves in steady and pseudo-steady flow with and without relaxation. *J. Fluid Mech.* **90**, 541–566.
- IVANOV, M. S., GIMELSHEIN, S. F., KUDRYAVTSEV, A. N. & MARKELOV, G. N. 1998a Transition from regular to Mach reflection in two- and three-dimensional flows. *Proc. 21st Intl Symp. Shock Waves, Great Keppel, Australia, 20–25 July 1997* (ed. A. F. P. Howing), vol. 2, P. 813. Panther.
- IVANOV, M. S., KLEMENKOV, G. P., KUDRYAVTSEV, A. N., NIKIFOROV, S. B., PAVLOV, A. A., FOMIN, V. M., KHARITONOV, A. M., KHOTYANOVSKY, D. V. & HORNUNG, H. G. 1998b Experimental and numerical study of the transition between regular and Mach reflections of shock waves in steady flows. *Proc. 21st Intl Symp. Shock Waves, Great Keppel, Australia, 20–25 July 1997*, vol. 2, P. 819, Panther.
- LI, H., CHPOUN, A. & BEN-DOR, G. 1999 Analytical and experimental investigations of the reflection of asymmetric shock waves in steady flows. *J. Fluid Mech.* **390**, 25–43.

- NEUMANN, J. VON 1945 Refraction, intersection and reflection of shock waves. *NAVORD Rep.* 203–45. Navy Dept., Bureau of Ordinance, Washington, DC, USA.
- ONOFRI, M. & NASUTI, F., 2001 Theoretical considerations on shock reflections and their implications on the evaluation of air intake performance. *Shock Waves* **11**, 151–156.
- SKEWS, B. W. 1997 Aspect ratio effects in wind tunnel studies of shock wave reflection transition. *Shock Waves* **7**, 373–383.
- SKEWS, B. W. 1998 Oblique shadowgraph study of shock wave reflection between two wedges in supersonic flow. *Book of Abstracts, 13th Intl Mach Reflection Symp., Beer Sheva, Israel.*
- SKEWS, B. W. 2000 Three-dimensional effects in wind tunnel studies of shock wave reflection. *J. Fluid Mech.* **407**, 85–104.
- VASILIEV, E. I. 1996 A W-modification of Godunov's method and its application to two-dimensional non-stationary flows of a dusty gas. *Comput. Math. Math. Phys.* **36**, 101–112. (Transl. from *Zh. Vychisl. Mat. Mat. Fiz.* **36**(1), 122–135.)
- VASILIEV, E. I. & KRAIKO, A. N. 1999 Numerical simulation of weak shock diffraction over a wedge under the von Neumann paradox conditions. *Comput. Math. Math. Phys.* **39**, 1335–1345. (Transl. from *Zh. Vychisl. Mat. Mat. Fiz.* **39**(8), 1393–1404.)